

J/Ψ production in two-photon collisions at next-to-leading order

L. Mihaila^{a*}

^aII. Institut für Theoretische Physik, Universität Hamburg,
Luruper Chaussee 149, 22761 Hamburg, Germany

In this paper, we report on the calculation of the cross section of J/Ψ plus jet inclusive production in direct $\gamma\gamma$ collisions at next-to-leading order within the factorization formalism of nonrelativistic quantum chromodynamics (NRQCD). Theoretical predictions for the future e^+e^- linear collider TESLA are also presented.

1. INTRODUCTION

Heavy quarkonium played an important role in establishing the asymptotic freedom of QCD, as its mass is much larger than the low-energy scale of the strong interactions Λ_{QCD} . On the other hand, the compensation of colour in heavy quarkonium gives new insights into the confinement mechanism, a nonperturbative process which is still not fully understood.

The factorization approach based on the non-relativistic QCD (NRQCD) [1,2] provides a rigorous and systematic framework for calculating perturbative and relativistic corrections to heavy quarkonium production and annihilation rates. This formalism implies a separation of short-distance coefficients, which can be expressed as perturbative expansions in the strong-coupling constant α_s , from the long-distance matrix elements (MEs), which must be extracted from the experiment. The MEs are predicted to scale with a definite power of the heavy quark relative velocity v . In this way, the theoretical calculations are organized as double expansions in α_s and v . Within the NRQCD formalism, the colour-octet (CO) processes contribute to the production and decay rates at some level. Their quantitative significance was assessed for inclusive charmonium hadroproduction observed at the Fermilab Tevatron [3]. However, it is necessary to test the universality of the MEs in other kinds of production

processes, such as $\gamma\gamma$ collisions. This process was studied at LEP2, where the photons originated from hard initial-state bremsstrahlung. Hopefully, the future e^+e^- linear collider will be built, for which an additional source of hard photons would be provided by beamstrahlung.

However, the leading-order theoretical predictions to be compared with the experimental data suffer from considerable uncertainties, mostly from the dependences on the renormalization and factorization scales and from the lack of information on the nonperturbative MEs. In this paper, we report on the calculation of the next-to-leading order (NLO) corrections to the inclusive production of J/Ψ mesons in $\gamma\gamma$ collisions. This is a first step in a comprehensive programme concerning the study of charmonium production at NLO within the NRQCD framework.

2. NLO CORRECTIONS TO J/Ψ DIRECT PHOTOPRODUCTION

In the following, we take into consideration the process $\gamma\gamma \rightarrow J/\Psi + j + X$, where X denotes the hadronic remnant possibly including a second jet. We restrict the analysis to j and X free of charm quarks and to finite values for the J/Ψ transverse momentum p_T . Two-photon processes can be modelled by assuming that each photon either interacts directly (direct photoproduction) or fluctuates into hadronic components (resolved photoproduction). Thus, the above mentioned process receives contributions from the direct, single-resolved, and double-resolved channels. Further-

*Talk given at International Conference and Loops and Legs in Quantum Field Theory, Zinnowitz, Germany, 25-30 April 2004.

more, we concentrate on the NLO calculation of the inclusive cross section for direct photoproduction.

At LO in α_s , there is only one partonic subprocess that scales like v^2 , namely

$$\gamma\gamma \rightarrow c\bar{c}[{}^3S_1^{(8)}] + g. \quad (1)$$

The representative Feynman diagrams together with the analytic expression of the LO cross section for the process (1) can be found in Ref. [4]. In the calculation of the production rates beyond LO in α_s , ultraviolet (UV), infrared (IR), and Coulomb divergences arise and need to be regularized. One of the most convenient method to handle the UV and IR singularities which are present in the short-distance coefficients as well as in the MEs is dimensional regularization. We introduce a 't Hooft mass μ and a factorization mass M as unphysical scales, and formally distinguish between UV and IR poles. The Coulomb singularities are regularized by assigning a small relative velocity between the c and \bar{c} quarks. For the extraction of the short-distance coefficients we apply the projector formalism of Refs. [5,6].

In the following, we study virtual and real radiative corrections separately, as their calculation requires different approaches.

2.1. Virtual Corrections

Feynman diagrams that generate the virtual corrections to the process (1) can be collected into two classes. The first one is obtained by attaching one virtual gluon in all possible ways to the tree-level diagrams. They include self-energy, triangle, box, and pentagon diagrams. Loop insertions in external gluon or c -quark lines are taken into consideration in the respective wave-function renormalization constants. The self-energy and triangle diagrams are in general UV divergent; the triangle, box and pentagon diagrams are in general IR divergent. The pentagon diagrams comprising only abelian gluon vertices also contain Coulomb singularities which cancel out similar poles in the radiative corrections to the operator $\langle \mathcal{O}^H[{}^3S_1^{(8)}] \rangle$. For the analytical treatment of the abelian five-point functions, we refer to Ref. [7].

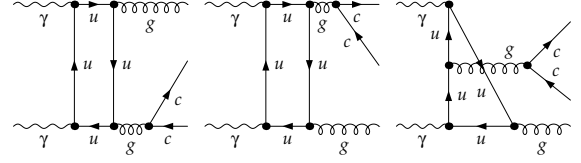


Figure 1. Light-quark box diagrams contributing to the virtual corrections to $\gamma\gamma \rightarrow c\bar{c}[{}^3S_1^{(8)}] + g$.

The diagrams of the second class comprise light-quark loops. The individual contributions arising from the triangle diagrams are equal to zero according to Furry's theorem [8]. The box diagrams, selectively shown in Fig. 1, contain UV and IR singularities, but their sum is finite.

The UV divergences comprised in self-energy and triangle diagrams are cancelled upon renormalization of the QCD gauge coupling $g_s = \sqrt{4\pi\alpha_s}$, the charm-quark mass m and field Ψ , and the gluon field A . We adopt the on-mass-shell (OS) scheme to renormalize m , Ψ , and A , while for g_s we employed the modified minimal-subtraction ($\overline{\text{MS}}$) scheme.

2.2. Operator Renormalization

For a consistent NLO analysis, one should also consider higher-order corrections in α_s to the four-quark operator $\langle \mathcal{O}^H[{}^3S_1^{(8)}] \rangle$ within NRQCD. This bare d -dimensional operator has mass dimension $d - 1$ while its renormalized version, which is extracted from the experimental data, has mass dimension 3. We thus introduce the 't Hooft mass scale of NRQCD, λ , to compensate for the difference between bare and renormalized operators. The corresponding tree-level and one-loop diagrams are depicted in Fig. 5 of Ref. [6]. Using dimensional regularization, the NRQCD Feynman rules in the quarkonium rest frame, and firstly expanding the integrands as Taylor series in $1/m$, and afterwards performing the integration over the loop momentum, we obtain the unrenormalized one-loop result

$$\begin{aligned} \langle \mathcal{O}^H[{}^3S_1^{(8)}] \rangle_1 &= \langle \mathcal{O}^H[{}^3S_1^{(8)}] \rangle_0 \\ &\times \left[1 + \left(C_F - \frac{C_A}{2} \right) \frac{\pi\alpha_s}{2v} \right] \end{aligned}$$

$$\begin{aligned}
& + \frac{4\alpha_s}{3\pi m^2} \left(\frac{4\pi\mu^2}{\lambda^2} \right)^\epsilon \exp(-\epsilon\gamma_E) \left(\frac{1}{\epsilon_{UV}} - \frac{1}{\epsilon_{IR}} \right) \\
& \times \left(\sum_{J=0}^2 C_F \langle \mathcal{O}^H [{}^3P_J^{(1)}] \rangle \right. \\
& \left. + \sum_{J=0}^2 B_F \langle \mathcal{O}^H [{}^3P_J^{(8)}] \rangle \right), \quad (2)
\end{aligned}$$

where the subscript 0 labels the tree-level quantity and μ is the 't Hooft mass scale of QCD. The presence of UV divergences indicates that the $\langle \mathcal{O}^H [{}^3S_1^{(8)}] \rangle$ operator needs renormalization. For this, we chose the $\overline{\text{MS}}$ scheme so that the $1/\epsilon_{UV}$ pole in Eq.(2) is cancelled out by the $1/\epsilon_{UV} + \ln(4\pi) - \gamma_E$ pole in the coefficient of the counterterm ME. The term proportional with $1/v$ represents the Coulomb singularity, which compensates a similar term in the virtual corrections. After the renormalization of the NRQCD ME and cancellation of the Coulomb singularity, an IR counterterm at $\mathcal{O}(\alpha_s)$ is generated from Eq.(2), which is indispensable to render the overall NLO result finite. This feature will be discussed in some detail in the next section.

2.3. Real Corrections

The real corrections to the process (1) arise from the partonic subprocesses

$$\gamma(k_1) + \gamma(k_2) \rightarrow c\bar{c}[n](p) + g(k_3) + g(k_4), \quad (3)$$

where $n = {}^3P_J^{(1)}, {}^1S_0^{(1)}, {}^1S_0^{(8)}, {}^3S_1^{(8)}, {}^3P_J^{(8)}$, and

$$\gamma(k_1) + \gamma(k_2) \rightarrow c\bar{c}[n](p) + q(k_3) + \bar{q}(k_4), \quad (4)$$

where $n = {}^1S_0^{(8)}, {}^3S_1^{(8)}, {}^3P_J^{(8)}$. For the respective Feynman diagrams we refer to Fig. 2 and Fig. 3 of Ref. [4]. Note that the colour-singlet states $n = {}^3S_1^{(1)}$ in process (3) and $n = {}^3P_J^{(1)}, {}^1S_0^{(1)}$ in process (4) are forbidden by the Furry's theorem [8] and colour conservation, respectively.

Integrating the squared MEs of the processes (3) and (4) over the three-particle phase space while keeping the value of p_T finite, we encounter IR singularities, which can be of the soft and/or collinear type. In order to systematically extract these singularities, it is useful to slice the phase space by introducing infinitesimal dimensionless cut-off parameters δ_i and δ_f , which are

connected with the initial and final states, respectively [9]. In the case of process (3) we distinguish *soft*, *final-state collinear* and *hard* regions of the phase space. In case of process (4) we differentiate *initial-state collinear* and *hard* regions of the phase space. While the individual contributions depend on the cut-off parameters δ_i or δ_f , their sum must be independent of them. We used the numerical verification of the cut-off independence as a check for our calculation.

The contributions originating from process (3) with $n = {}^3S_1^{(8)}$ contain IR (soft and final-state collinear) singularities which cancel out singularities of the same type comprised in the virtual corrections, as required by the Kinoshita-Lee-Nauenberg theorem [10]. The subprocesses with $n = {}^3P_J^{(1)}, {}^3P_J^{(8)}$ generates contributions containing only soft divergences. These are cancelled out by the IR poles leftover in the renormalized $\langle \mathcal{O}^H [{}^3S_1^{(8)}] \rangle$ operator, which organise themselves as coefficients of the $\langle \mathcal{O}^H [{}^3P_J^{(1,8)}] \rangle$ operators.

According to the mass factorization theorem [11], the form of the collinear singularities present in the squared amplitudes of processes (4), which are related with an incoming-photon leg, is universal and the pole can be absorbed into the bare PDF of the antiquark \bar{q} inside the resolved photon. As a consequence, the real MEs acquire an explicit dependence on the mass factorization scale M . In turn, the resolved-photon contribution is evaluated with the renormalized photon PDF, which are also M dependent. In the sum of these two contributions, the M dependence cancels up to terms beyond NLO.

3. PHENOMENOLOGICAL STUDY

In the following, we study the phenomenological significance of the process

$\gamma\gamma \rightarrow J/\Psi + j + X$ at TESLA in its e^+e^- mode, with $\sqrt{s} = 500$ GeV and the photon sources bremsstrahlung and beamstrahlung coherently superposed. For the energy spectrum of the photons we refer to Eq. (27) of Ref. [12] and Eq. (2.14) of Ref. [13], and for the designed experimental parameters to Ref. [14] and Ref. [15],

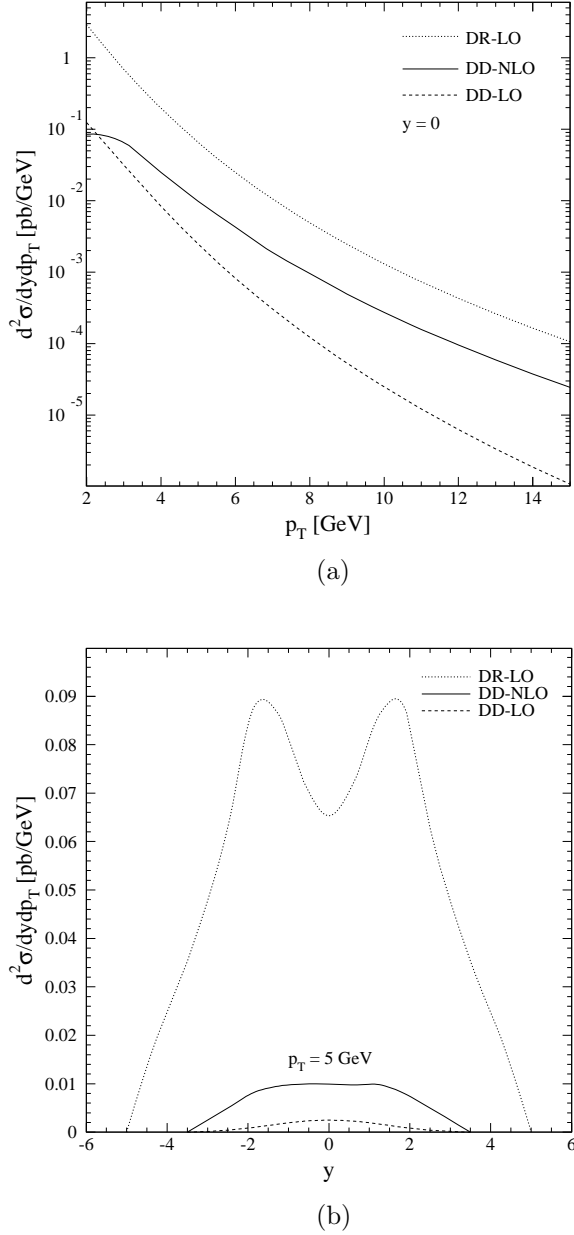


Figure 2. Differential cross section $d^2\sigma/dp_T dy$ of $e^+e^- \rightarrow e^+e^- J/\psi + X$ at TESLA with $\sqrt{s} = 500$ GeV (a) for $y = 0$ as a function of p_T and (b) for $p_T = 5$ GeV as a function of y .

respectively.

We use $m = 1.5$ GeV, $\alpha = 1/137.036$, and the two-loop formula for $\alpha_s^{(n_f)}(\mu)$ [16] with $n_f = 3$ active quark flavours and $\Lambda_{\text{QCD}}^{(3)} = 299$ MeV [17]. As for photon PDFs, we employ the NLO set from Gluück, Reya, and Schienbein (GRS) [17], which are implemented in the fixed fixed-flavour-number scheme, with $n_f = 3$. Our default choice of renormalization and factorization scales is $\mu = M = m_T$ and $\lambda = m$. As for J/ψ , χ_{cJ} , and ψ' MEs, we adopt the LO sets determined in Ref. [18] using the LO set of proton PDFs from Martin, Roberts, Stirling, and Thorne (MRST98LO) [19].

In Fig. 2, we study $d^2\sigma/dp_T dy$ (a) for $y = 0$ as a function of p_T and (b) for $p_T = 5$ GeV as a function of y . The solid and dashed lines represent NLO and LO results, respectively, for the direct photoproduction. The dotted lines correspond to LO result of the single-resolved photoproduction evaluated with the LO versions of the $\alpha_s^{(n_f)}(\mu)$ and the photon PDFs. Notice that we do not consider p_T values smaller than 2 GeV, where additional IR singularities occur.

From Fig. 2(a), we observe that, the NLO result of direct photoproduction falls off with increasing p_T more slowly than LO one. This feature may be accounted for by the *fragmentation-prone* partonic subprocesses that contribute at NLO result, while they are absent at LO. Such subprocesses contain a gluon with a small virtuality that splits into a $c\bar{c}$ pair in the Fock state $n = {}^3S_1^{(8)}$. They generally provide dominant contributions at $p_T \gg 2m$ due to the presence of a large gluon propagator. In single-resolved photoproduction, a fragmentation-prone partonic subprocess already contributes at LO. This explains why the solid and dotted curves in Fig. 2(a) run parallel in the upper p_T range. In the lower p_T range, the fragmentation-prone partonic subprocesses do not matter, as the gluon propagator becomes finite and the Fock state $n = {}^3S_1^{(8)}$ is already present at LO.

As one can notice from Fig. 2(b), at $p_T = 5$ GeV, single-resolved photoproduction is still overwhelming. The two pronounced maxima of the LO single-resolved result may be explained

by the occurrence of a virtual gluon in a t channel that can be almost collinear with the incoming quark q or by the one of a virtual quark in the u channel that can become almost collinear with the incoming photon. The NLO result increases towards forward and backward directions due to the finite reminders of the initial-state collinear singularities that were absorbed into the photon PDFs.

4. CONCLUSIONS

The experimental verification of the NRQCD factorization hypothesis is of great importance especially for charmonium, because the charm quark mass might not be large enough to justify the nonrelativistic approximation.

In this paper, we studied at NLO the inclusive production of prompt J/Ψ mesons with finite values of p_T . This is the first time that an inclusive $2 \rightarrow 2$ production process was treated at NLO within the NRQCD factorization formalism. A complete NLO calculation of prompt J/Ψ production in $\gamma\gamma$ collisions allows a NLO treatment of photo and hadroproduction as well. This will provide a solid basis for the attempt to accommodate the NRQCD theoretical predictions with the experimental data to be taken at high-energy colliders, such as the Tevatron (RunII) and HERA (HERA-II).

Acknowledgements

The author thanks M. Klasen, B.A. Kniehl, and M. Steinhauser for a fruitful collaboration.

REFERENCES

1. W.E. Caswell, G.P. Lepage, Phys. Lett. B 167 (1986) 437.
2. G.T. Bodwin, E. Braaten, G.P. Lepage, Phys. Rev. D 51 (1995) 1125; *ibid.* 55 (1997) 5853, Erratum.
3. CDF Collaboration, F. Abe et al., Phys. Rev. Lett. 69 (1992) 3704; *ibid.* 71 (1993) 2537; *ibid.* 79 (1997) 572; *ibid.* 79 (1997) 578; D0 Collaboration, S. Abachi et al., Phys. Lett. B 370 (1996) 239; D0 Collaboration, B. Abbott et al., Phys. Rev. Lett. 82 (1999) 35.
4. M. Klasen, B.A. Kniehl, L.N. Mihaila, M. Steinhauser, Nucl. Phys. B 609 (2001) 518.
5. J. Kaplan, J.H. Kühn, Phys. Lett. B 78 (1978) 252.
6. A. Petrelli, M. Cacciari, M. Greco, F. Maltoni, M.L. Mangano, Nucl. Phys. B 514 (1998) 245.
7. W. Beenakker, S. Dittmaier, M. Krämer, B. Plümper, M. Spira, P.M. Zerwas, Nucl. Phys. B 653 (2003) 151.
8. W.H. Furry, Phys. Rev. 51 (1937) 125.
9. K. Fabricius, G. Kramer, G. Schierholz, I. Schmitt, Z. Phys. C 11 (1981) 315; B.F. Harris, J.F. Owens, Phys. Rev. D 65 (2002) 094032.
10. T. Kinoshita, J. Math. Phys. 3 (1962) 650; T.D. Lee, M. Nauenberg, Phys. Rev. B 133 (1964) 1549.
11. R.J. DeWitt, L.M. Jones, J.D. Sullivan, D.E. Willen, H.W. Wyld, Jr., Phys. Rev. D 19 (1979) 2046; *ibid.* 20 (1979) 1751, Erratum.
12. S. Frixione, M.L. Mangano, P. Nason, G. Ridolfi, Phys. Lett. B 319 (1993) 339.
13. P. Chen, T.L. Barklow, M.E. Peskin, Phys. Rev. D 49 (1994) 3209.
14. J. A. Aguilar-Saavedra et al., in: R.-D. Heuer, D. Miller, F. Richard, P. Zerwas (Eds.), TESLA Technical Design Report, Part III, p. III-166.
15. J. Andruszkow et al., in: R. Brinkmann, K. Flöttmann, J. Rossbach, P. Schmüser, N. Walker, H. Weise (Eds.), TESLA Technical Design Report, Part II, p. II-1.
16. Particle Data Group, K. Hagiwara et al., Phys. Rev. D 66 (2002) 010001.
17. M. Glück, E. Reya, I. Schienbein, Phys. Rev. D 60 (1999) 054019; *ibid.* 62 (1999) 019902, Erratum.
18. E. Braaten, B.A. Kniehl, J. Lee, Phys. Rev. D 62 (2000) 094005.
19. A.D. Martin, R.G. Roberts, W.J. Stirling, R.S. Thorne, Eur. Phys. J. C 4 (1998) 463.